ACS APPLIED MATERIALS & INTERFACES

Research Article

www.acsami.org

Polyethylenimine (PEI) As an Effective Dopant To Conveniently Convert Ambipolar and p-Type Polymers into Unipolar n-Type Polymers

Bin Sun,[†] Wei Hong,[†] Emmanuel S. Thibau,[‡] Hany Aziz,[§] Zheng-Hong Lu,[‡] and Yuning Li*[,†]

[†]Department of Chemical Engineering and [§]Department of Electrical and Computer Engineering, Waterloo Institute for Nanotechnology (WIN), University of Waterloo, 200 University Avenue West, Waterloo, Ontario N2L 3G1, Canada

[‡]Department of Materials Science and Engineering, University of Toronto, 184 College Street, Toronto, Ontario M5S 3E4, Canada

Supporting Information

ABSTRACT: In this study, we added a small amount of polyethylenimine (PEI) into several ambipolar and p-type polymer semiconductors and used these blends as channel materials in organic thin film transistors (OTFTs). It is found that PEI can effectively suppress hole transport characteristics while maintaining or promoting the electron transport performance. Unipolar n-channel OTFTs with electron-only transport behavior is achieved for all the polymer semiconductors chosen with 2−10 wt % PEI. The electron-rich nitrogen atoms in PEI are thought to fill the electron traps, raise the Fermi level and function as trapping sites for holes, leading to promotion of electron transport and suppression of hole transport. This work demonstrates a convenient general approach to transforming ambipolar and p-type polymer semiconductors into unipolar n-type polymer semiconductors that are useful for printed logic circuits and many other applications.

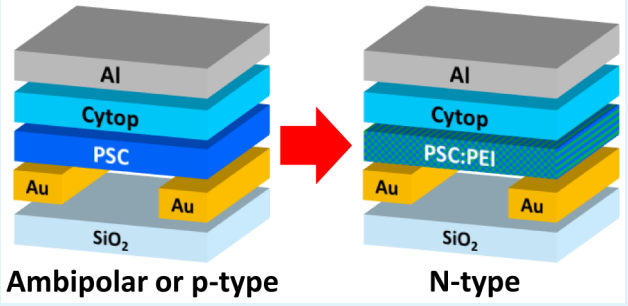

KEYWORDS: *ambipolar, n-type, polarity conversion, polymer semiconductors, organic thin film transistors*

1. INTRODUCTION

Intensified efforts have been made in recent years to develop π-conjugated polymers consisting of alternating electron donor (D) and acceptor (A) units in their backbone for organic photovoltaics (OPVs)[1−7] and organic thin film transistors (OTFTs)[6−9] to achieve performances approaching or exceeding those of certain inorganic counterparts. For example, OPVs based on D−A polymers have reached power conversion efficiencies greater than 10%,[10] while OTFTs using D−A polymers have demonstrated field effect mobility values in the excess of 10 $cm^2\ V^{-1}\ s^{-1}$.[11−13] For many applications, the complementary metal oxide semiconductor (CMOS) logic is desirable because of a number of advantages such as high reliability, high signal robustness, and low power consumption.[14,15] To fabricate a CMOS-like logic circuit using OTFTs, both p-channel and n-channel OTFTs are required. Although many D−A polymers have been successfully used as hole transport semiconductors in p-channel OTFTs, very few have shown unipolar electron-only charge transport performance for use in unipolar n-channel OTFT devices.[6−9,16]

Because of the combination of the electron donor and acceptor units, a large number of D−A polymers have a rather narrow band gap (or closely positioned HOMO and LUMO levels), which facilitates the injection and transport of both holes and electrons, and thus exhibit ambipolar charge transport performance in OTFTs.[6,9,17−24] Although ambipolar polymers have been used in light-emitting transistors and CMOS-like circuits,[25] a very high standby current between the source and drain contacts is observed in these devices.[26]

Ambipolar organic semiconductors can be converted into unipolar materials by changing packing motif, which can be realized by side chain design,[27] thermal annealing,[28] and choice of the processing solvent.[29] Surface modification of the source and drain contacts with Ba or Cs salts,[30,31] organic thiols and polyethylenimine[32] has been used as a strategy to reduce the work function (or raise the Fermi energy) of the electrodes and facilitate electron injection of small molecule or polymer semiconductors in OTFTs. Very recently, we reported a successful conversion of ambipolar and p-type OTFTs based on several D−A polymers into unipolar n-type OTFTs[33,34] by depositing a thin layer (∼2−5 nm) of polyethylenimine (PEI, Figure 1) on the Au source/drain contacts. The work function of the PEI-modified Au could be dramatically reduced from 5.1 eV to as low as 3.2 eV.[32,33] It was thought that such a low work function could build up a large energy barrier to block hole injection and facilitate electron injection. Another effective way to suppress the hole transport and promote the electron transport of small molecule or polymer semiconductors is n-

Received: June 9, 2015
Accepted: August 5, 2015
Published: August 5, 2015

DOI: 10.1021/acsami.5b05097
ACS Appl. Mater. Interfaces 2015, 7, 18662−18671

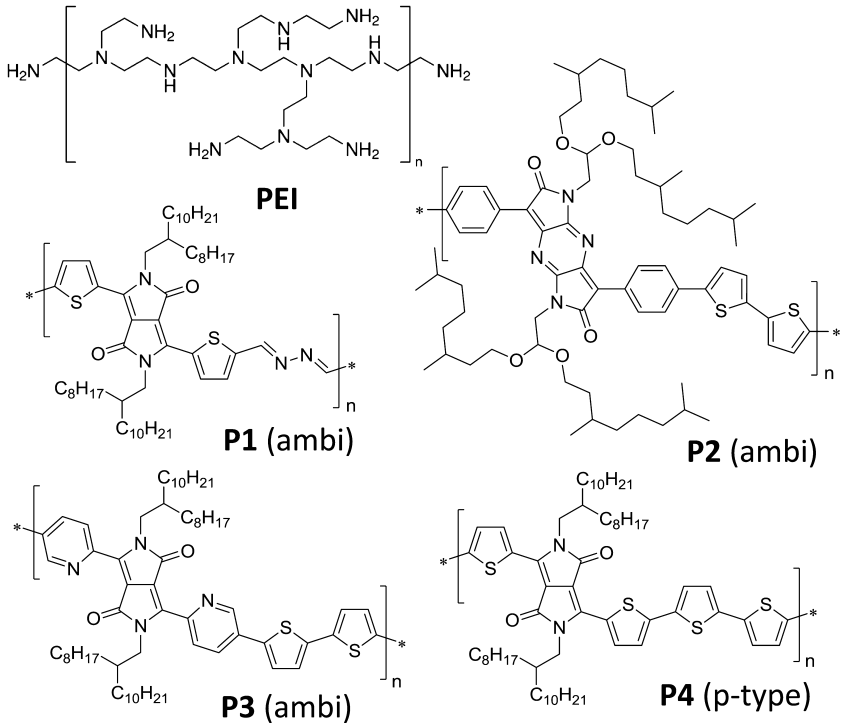

Figure 1. Chemical structures of PEI (branched polyethylenimine) and polymer semiconductors PDBTAZ (**P1**)[21] (E_{HOMO}/E_{LUMO} = −5.67 eV/−4.24 eV), PPzDPDP-BT (**P2**)[24] (E_{HOMO}/E_{LUMO} = −5.59 eV/−4.17 eV), PDBPyBT (**P3**)[22] (E_{HOMO}/E_{LUMO} = −5.69 eV/−4.33 eV), and PDQT (**P4**)[42,52] (E_{HOMO}/E_{LUMO} = −5.24 eV/−4.04 eV) used in this study. **P1**, **P2**, and **P3** were previously reported to show typical ambipolar (ambi) charge transport performance, whereas **P4** showed typical p-type hole-only transport performance when gold was used as source/drain contacts in an OTFT device.

type doping with cobaltocenes,[35,36] small molecule amine compounds[37−40] or CsF.[36,41] In this study, we successfully demonstrate that PEI is also a very effective polymeric dopant to convert ambipolar and even p-type D−A polymer semiconductors (PSCs) into high-performance unipolar n-type polymers in OTFTs. PEI and these PSCs are readily miscible in a common solvent to form homogeneous solutions, which can be spin-coated into smooth blend films with uniformly distributed PEI at the nanoscale.

2. EXPERIMENTAL SECTION

Materials and Methods. PEI (branched polyethylenimine with an M_w of ∼25 000 by light scattering and an M_n of 10 000 by GPC) was purchased from Sigma-Aldrich. Cytop (a fluoropolymer of Asahi Glass Co., Ltd.) was purchased from Bellex International Corporation. All other chemicals were obtained from commercial sources and used without further purification. Ambipolar polymers, PDBTAZ (**P1**)[21] (M_n = 102 000, PDI (polydispersity index) = 4.30), PPzDPDP-BT (**P2**)[24] (M_n = 27 500, PDI = 2.84), PDBPyBT (**P3**)[22] (M_n = 26 300, PDI = 3.56), and a p-type polymer, PDQT (**P4**)[42] (M_n = 40 000, PDI = 3.22), used in this study were synthesized and reported previously. Ultraviolet−visible−near-infrared (UV−vis−NIR) spectroscopy measurements of polymer thin films spin-coated on quartz were performed on a PerkinElmer Lambda 1050 UV/vis/NIR spectrophotometer. The X-ray diffractometry (XRD) measurements of the polymer thin films spin-coated on Si/SiO_2 substrates were carried out on a Bruker D8 Advance diffractometer with Cu Kα1 radiation (λ = 1.5406 Å) in Bragg geometry. Atomic force microscopy (AFM) images of polymer thin films spin-coated on Si/SiO_2 substrates were obtained by a Dimension 3100 scanning probe microscope.

Time-of-Flight Secondary Ion Mass Spectrometry (TOF-SIMS) Measurement. A one-side polished, 500 μm thick heavily n-doped Si(100) (n^{++}-Si) substrate with a resistivity of 0.1−0.01 Ohm cm was cleaned by RCA 1 (H_2O_2−NH_4OH-H_2O) and then rinsed in buffered HF for 1 min to remove any SiO_2 present on its surface. A 20 nm Au layer (with 3 nm of Cr as a bottom adhesion layer) was thermally deposited on the polished side of the n^{++}-Si substrate. A polymer film was then deposited on the substrate by spin-coating a polymer solution and then drying on a hot plate at 150 °C for 15 min. TOF-SIMS depth profiles of the polymer film were obtained using an ION-TOF 5 system (IONTOF GmbH) in the spectrometry mode (noninterlaced) with a reflection time-of-flight analyzer operated in the negative polarity mode with a Bi^{3+} analysis ion source (30 kV), cycle time of 200 μs, and sampling area of 150 × 150 μm^2.[43] The sample was sputtered with Ar cluster ions (Ar_{1000}^+) at ion beam energy of 5 keV over an area of 400 × 400 μm^2. The TOF-SIMS spectra were mass-calibrated on carbon fragments (C_x). The species with mass-to-charge ratio (m/q) equal to 40 (corresponding to $C_2H_2N^-$), 12 (corresponding to C^-), and 197 (corresponding to Au^-) were used for detailed analysis.

Ultraviolet Photoelectron Spectroscopy (UPS) Measurement. A polymer semiconductor (with or without 2 wt % PEI) solution in chloroform (1 mg mL^{-1}) was spin-coated on a 30 nm Au film coated on n^{++}-Si substrate to form a film, followed by annealing at 150 °C for 15 min in nitrogen. UPS measurements were performed in a PHI5500 Multi-Technique system with a base pressure of $\sim 10^{-9}$ Torr and the Fermi energy calibrated to 0 eV. A helium discharge source (HeI α, hv =21.22 eV) was used and the samples were kept at a takeoff angle of 88°. During measurement, the sample was held at a −15 V bias relative to the spectrometer in order to efficiently collect low-kinetic energy electrons. Fermi level (E_F) was calculated from the equation: E_F = 21.22 eV − SEC, where SEC is the secondary electron cut-off. The difference between HOMO level and Fermi level, η, was determined from HOMO onset in the HOMO region.[44]

OTFT Device Fabrication. OTFT devices were fabricated on n^{++}-Si wafer substrate with a 300 nm-thick thermally grown SiO_2 layer. Au source and drain electrodes (40 nm thick) with a Cr adhesion layer (3 nm) were thermally deposited on the substrate using a conventional photolithography method. The substrate with source and drain pairs

DOI: 10.1021/acsami.5b05097
ACS Appl. Mater. Interfaces 2015, 7, 18662−18671

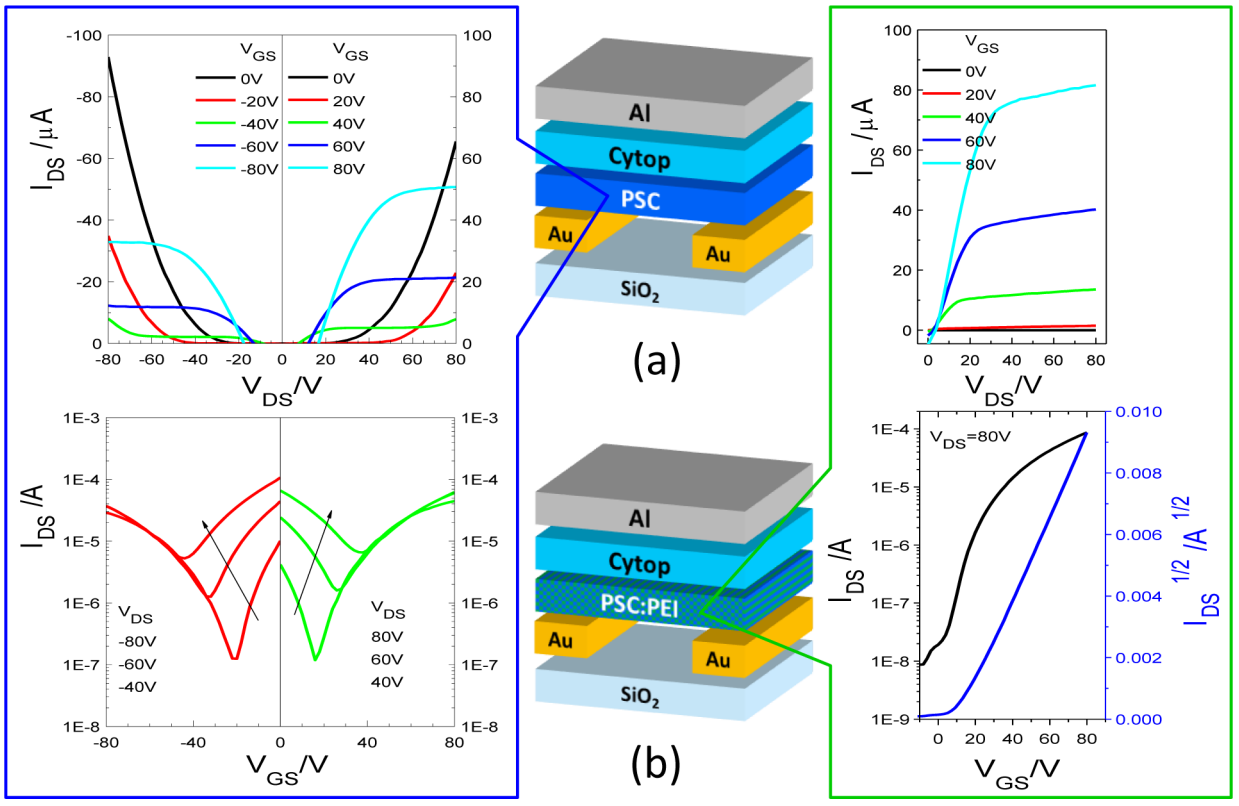

Figure 2. (a) TGBC OTFT device structure with a pristine polymer semiconductor (PSC) as the channel, Cytop as the gate dielectric, Al as the gate electrode and Au as the source and drain contacts; the output (upper) and transfer (lower) curves were obtained when an ∼40−50 nm thick pristine **P1** film (annealed at 150 °C) was used as the channel, which shows typical ambipolar charge transport performance. (b) TGBC OTFT device structure similar to that in (a) except that the channel is a PSC:PEI blend film; the output (upper) and transfer (lower) curves were obtained when a ∼ 40 nm thick **P1**:PEI (2% PEI) blend film (annealed at 150 °C) was used as the channel, which shows typical n-channel electron-only transport performance. Dimensions of all devices: channel length L = 30 μm; channel width W = 1 mm.

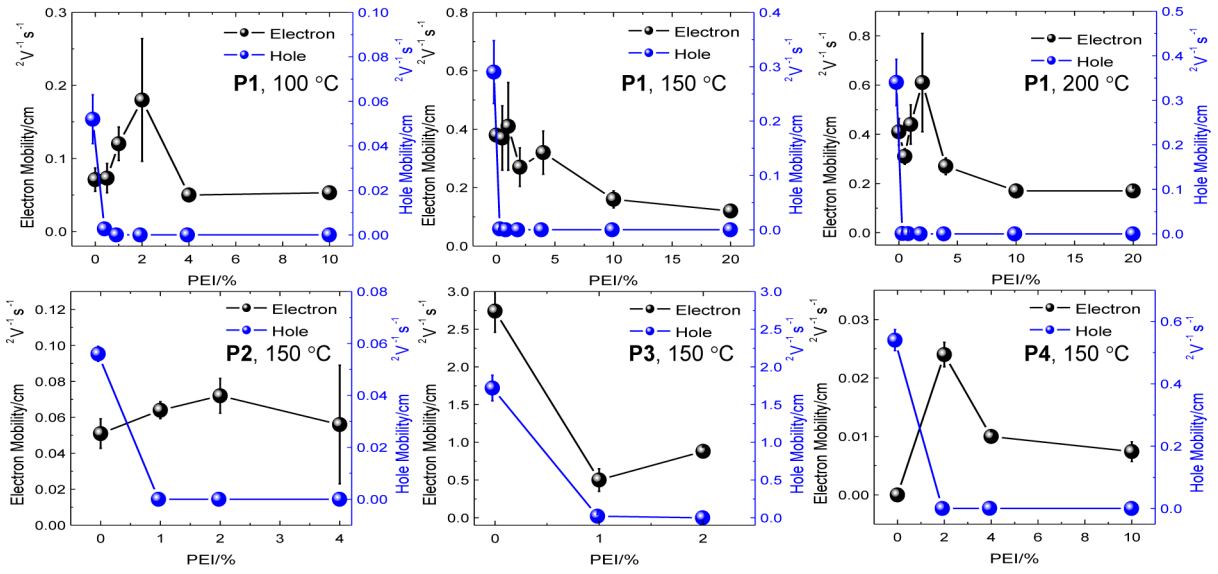

Figure 3. Dependence of hole and electron mobilities of **P1**−**P4** in OTFT devices on PEI content in the PSC:PEI blends. The PSC or PSC:PEI blend films were annealed at 100, 150, or 200 °C.

was cleaned sequentially with air plasma, acetone and isopropanol before being dried under a nitrogen flow.

Top-Gate Bottom-Contact (TGBC) Devices with Structure (a) (Figure 2a). A polymer semiconductor (PSC) solution in chlorobenzene (5 mg mL^{-1} for **P1**), chloroform (10 mg mL^{-1} for **P3**) or a mixture (9/1, v/v) of chloroform and 1,2-dichlorobenzene (DCB) (5 mg mL^{-1} for **P2** and **P4**) was spin-coated on the cleaned substrate to form a film with thickness of ∼40−50 nm and then annealed at 100, 150, or 200 °C for 15 min in nitrogen. Then Cytop (∼570 nm with C_i = 3.2 nF cm^{-2}) as the gate dielectric layer was deposited on the PSC by spin-coating, followed by drying on a hot plate at 100 °C for 1 h. Finally, an Al layer with a thickness of 70 nm was thermally deposited as the gate electrode. The device performance

DOI: 10.1021/acsami.5b05097
ACS Appl. Mater. Interfaces 2015, 7, 18662−18671

Table 1. TGBC OTFT Performance of Devices with Pristine PSC (PEI = 0 wt %) or PSC:PEI Blend Films As Channel Semiconductors[a]

polymer	PEI (wt %)	$T_{Ann.}$[b] (C)	$\mu_{e,max}$[c] ($cm^2 V^{-1} s^{-1}$)	$\mu_{e,aye}$ (std[d]) ($cm^2 V^{-1} s^{-1}$)	$\mu_{h,max}$[e] ($cm^2 V^{-1} s^{-1}$)	$\mu_{h,ave}$ (std) ($cm^2 V^{-1} s^{-1}$)	V_{th}[f] (V)	I_{on}/I_{off}[g]
P1	0	100	0.088	0.071 (0.016)	0.060	0.052 (0.011)		
		150	0.40	0.38 (0.016)	0.29	0.29 (0.0058)		
		200	0.47	0.41 (0.054)	0.41	0.33 (0.052)		
	0.5	100	0.097	0.073 (0.020)	0.007	$\sim 2.7 \times 10^{-3}$		
		150	0.55	0.37 (0.11)	0.005	$\sim 1.7 \times 10^{-3}$		
		200	0.37	0.31 (0.032)	0.002	$\sim 8.6 \times 10^{-4}$		
	1	100	0.16	0.12 (0.023)		none	2	$\sim 1 \times 10^2$ to $\sim 1 \times 10^3$
		150	0.64	0.41 (0.15)		none	20	$\sim 1 \times 10^3$
		200	0.56	0.44 (0.093)		$\sim 1 \times 10^{-3}$	28	$\sim 1 \times 10^2$ to $\sim 1 \times 10^3$
	2	100	0.34	0.18 (0.084)		none	9	$\sim 1 \times 10^4$ to $\sim 1 \times 10^5$
		150	0.38	0.27 (0.076)		none	12	$\sim 1 \times 10^3$ to $\sim 1 \times 10^4$
		200	0.88	0.61 (0.20)		none	21	$\sim 1 \times 10^3$ to $\sim 1 \times 10^4$
	4	100	0.063	0.050 (0.0094)		none	−5	$\sim 1 \times 10^3$ to $\sim 1 \times 10^4$
		150	0.39	0.32 (0.085)		none	12	$\sim 1 \times 10^3$ to $\sim 1 \times 10^4$
		200	0.30	0.27 (0.034)		none	22	$\sim 1 \times 10^3$ to $\sim 1 \times 10^4$
	10	100	0.068	0.053 (0.0089)		none	0	$\sim 1 \times 10^1$ to $\sim 1 \times 10^2$
		150	0.21	0.16 (0.029)		none	8	$\sim 1 \times 10^2$ to $\sim 1 \times 10^3$
		200	0.21	0.17 (0.028)		none	20	$\sim 1 \times 10^3$ to $\sim 1 \times 10^4$
	20	150	0.15	0.12 (0.022)		none	8	$\sim 1 \times 10^2$
		200	0.18	0.17 (0.011)		none	21	$\sim 1 \times 10^3$ to $\sim 1 \times 10^4$
P2	0	150	0.063	0.051 (0.0082)	0.098	0.056 (0.0029)		
	1	150	0.071	0.064 (0.0047)		$\sim 1 \times 10^{-5}$	24	$\sim 1 \times 10^3$
	2	150	0.084	0.072 (0.0097)		none	22	$\sim 1 \times 10^3$
	4	150	0.060	0.056 (0.033)		none	23	$\sim 1 \times 10^3$
P3	0	150	3.13	2.74 (0.28)	1.93	1.72 (0.17)		
	1	150	0.73	0.50 (0.15)	0.05	0.020 (0.024)		
	2	150	0.95	0.88 (0.058)		none	4	$\sim 1 \times 10^2$ to $\sim 1 \times 10^3$
P4	0	150	none	none	0.58	0.54 (0.034)	−12	$\sim 1 \times 10^3$
	2	150	0.027	0.024 (0.0021)	2.7×10^{-5}	$\sim 1.3 \times 10^{-5}$	37	$\sim 1 \times 10^2$
	4	150	0.011	0.010 (8.2×10^{-4})	9.4×10^{-4}	$\sim 3.9 \times 10^{-4}$	31	$\sim 1 \times 10^2$
	10	150	0.010	0.0074 (0.0017)		none	39	$\sim 1 \times 10^2$ to $\sim 1 \times 10^3$

[a]Data were obtained from at least five devices for each condition. [b]Annealing temperature. [c]Electron mobility measured at V_{DS} = 80 V. [d]Standard deviation. [e]Hole mobility measured at V_{DS} = −80 V. [f]Threshold voltage. [g]Current on-to-off ratio.

was characterized in air in the absence of light using an Agilent 4155C Analyzer. The carrier mobility was calculated from the slope of the $(I_{DS})^{1/2}$ versus V_{GS} plot in the saturation regime according to the equation: $I_{DS} = \mu C_i W/(2L) (V_{GS}-V_{TH})^2$, where μ is the saturation mobility, I_{DS} is the drain current, C_i is the gate dielectric layer capacitance per unit area, L (30 μm) and W (1 mm) are the channel length and width, respectively, and V_{GS} and V_{TH} are the gate and threshold voltages, respectively.

TGBC Devices with Structure (b) (Figure 2b). The devices were fabricated and characterized following the similar procedure described for devices with structure (a) except that a PSC:PEI mixture solution was used to make the PSC:PEI blend layer. A mixture of PSC:PEI in a certain ratio was dissolved in chlorobenzene (for **P1**), chloroform (for **P3**) or a mixture (9/1, v/v) of chloroform and DCB (for **P2** and **P4**) by stirring at 45 °C for 1 h before cooling to room temperature.

Dual-Gate Devices (Figure 7). The devices were fabricated and characterized following the similar procedures described for devices with structure (a) except that a PEI layer (~1.5 nm) was deposited on top of the PSC (**P1**) layer by spin-coating a PEI solution (0.062 mg mL^{-1}) in IPA. The thickness of the PSC layer was ~85 nm. These dual-gate devices contain TGBC and bottom-gate bottom-contact (BGBC) configurations.

BGBC Devices (Figure S12). A solution of **P1** in chlorobenzene (5 mg mL^{-1}) was spin-coated on the cleaned substrate to form a polymer film with a thickness of ~40−50 nm, followed by annealing at 150 °C for 15 min in nitrogen.

3. RESULTS AND DISCUSSION

The chemical structures of four D−A polymers **P1**−**P4** used in this study are shown in Figure 1. These polymers have deep LUMO levels of $\lesssim -4$ eV (shown in Figure 1 caption), which are desirable for stable electron transport.[45,46] To evaluate the charge-transport performance of these polymers, we adopted the following top-gate bottom-contact (TGBC) OTFT configuration: Au as the source and drain contacts, Cytop as the gate dielectric, and Al as the top gate electrode (Figure 2). A Si wafer with a 300 nm thick thermally grown SiO_2 was used as the supporting substrate.

Pristine **P1** showed typical ambipolar charge transport behavior with balanced electron and hole mobilities at different annealing temperatures (Figures 2a and 3 and Table 1). The best average electron and hole mobilities ($\bar{\mu}_e$ and $\bar{\mu}_h$) are 0.41 and 0.33 $cm^2 V^{-1} s^{-1}$, respectively, achieved for the films annealed at 200 °C. Then we dissolved PEI and **P1** in chlorobenzene to form a solution containing 0.5% of PEI (wt % relative to the amount of the polymer semiconductor), which was then deposited as a blend film by spin-coating. TGBC OTFTs with these **P1**:PEI blend films exhibited similar $\bar{\mu}_e$ but significantly lower $\bar{\mu}_h$ (down to $\sim 1 \times 10^{-3}$ $cm^2 V^{-1} s^{-1}$) compared with pristine **P1** at all annealing temperatures. When the PEI content was increased to 1%, films annealed at 200 °C

DOI: 10.1021/acsami.5b05097
ACS Appl. Mater. Interfaces 2015, 7, 18662−18671

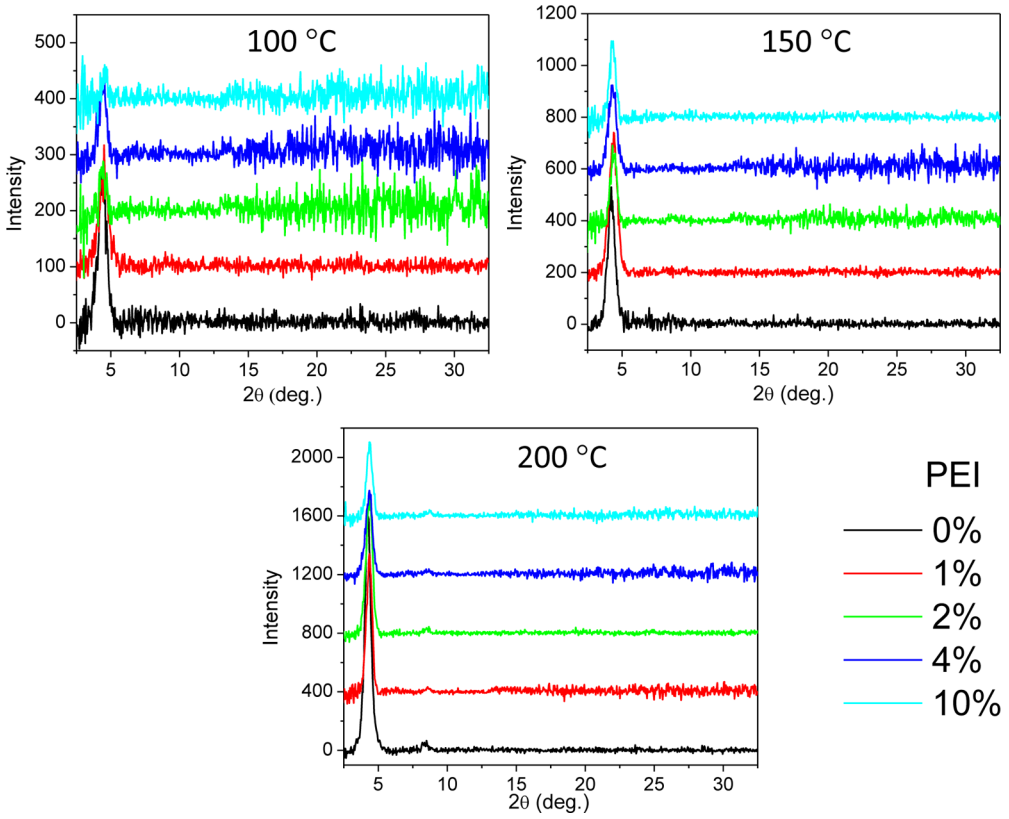

Figure 4. Out-of-plane XRD patterns of spin-coated thin films of **P1** with different PEI contents (wt % over **P1**) on bare SiO_2/Si substrates annealed at different temperatures measured in a reflection mode using Cu Kα1 radiation.

showed very weak hole transport characteristics, while those annealed at 100 °C and 150 °C exhibited electron-only charge transport performance with slightly improved electron mobility values. When 2% PEI was added, hole transport was completely suppressed in all devices, whereas the electron mobility was further enhanced in most of the cases. The largest electron mobility of 0.88 $cm^2\ V^{-1}\ s^{-1}$ was achieved in a unipolar n-channel device with a 200 °C-annealed film, which is much higher than the best electron mobility of the ambipolar devices with a pristine **P1** film (0.47 $cm^2\ V^{-1}\ s^{-1}$, Table 1) and the n-channel devices with PEI-modified Au contacts (0.53 $cm^2\ V^{-1}\ s^{-1}$).[33,34] With a further increase in the PEI content to 4, 10, and 20%, the electron mobility decreased gradually, but moderate values up to 0.18 $cm^2\ V^{-1}\ s^{-1}$ were still retained even when 20% PEI was added. It should be mentioned that **P1** (and **P2**−**P4**) and PEI could be dissolved at any blend ratio in a common solvent such as chlorobenzene, chloroform or a mixture of chloroform and 1,2-dichlorobenzene (DCB) to form a homogeneous solution. (The solution could be easily filtered through a 0.2 μm syringe filter.)

XRD patterns of the **P1**:PEI blend thin films with 1% PEI showed no or only a slight decrease in crystallinity in comparison to the pristine **P1** film at various annealing temperatures (Figure 4). When 2% PEI was added, the crystallinity of the blend film started to decrease. At 10% PEI, the crystallinity of the 100 °C-annealed film became very poor, indicating that the ordering of **P1** polymer chains was impeded by the PEI molecules. At higher temperatures, however, the films became quite crystalline.

Time-of-flight secondary ion mass spectrometry (TOF-SIMS) is a powerful technique to determine the chemical composition of a surface within a depth of 1 to 2 nm. We utilized TOF-SIMS to shed light on the vertical distribution of PEI in the **P1**:PEI blend thin films, since accumulation of PEI on the substrate in the TGBC devices (Figure 2) would reduce the work function of Au source and drain contacts to influence the charge injection (a detailed discussion will be made later). For comparison, three polymer thin films, PEI, **P1**, and **P1**:PEI (2% PEI) were deposited on Au coated n^{++}- Si substrates and annealed at 150 °C for 15 min in nitrogen prior to the TOF-SIMS measurement (Figure 5a). Argon gas cluster ions (Ar_{1000}^+) were used as the primary ions to sputter the polymer films.

Among many secondary ion species detected for the PEI film, $C_2H_2N^-$ was chosen for analysis because of its suitable signal intensity and appropriate mass for differentiating it from other ion species. For the pristine **P1** film, $C_2H_2N^-$ ions were also observed because this polymer contains C, H, and N atoms. Nonetheless, because $C_2H_2N^-$ signals for **P1** were about 2 orders of magnitude weaker than those of PEI, analysis of this ion species can still serve our purpose to study the vertical distribution of PEI in the **P1**:PEI film. Because the intensity of ion signals is significantly influenced by the experimental conditions, a comparison of the absolute $C_2H_2N^-$ ion counts between different polymer samples is inappropriate. Therefore, we used the C^- ion species generated from each sample as an internal reference and used the more reproducible $C_2H_2N^-/C^-$ ratio (the left *Y*-axis in Figure 5b) to plot the depth profiles. In addition, to determine the position of the polymer/Au interface (the top surface of the Au film), Au^- ions were also analyzed (the right *Y*-axis in Figure 5b). The vertical dashed line shown in Figure 5b represents the etching position where the Au^- ions start to increase, indicating that the primary ion beam had etched away the polymer film and reached the Au film's top

DOI: 10.1021/acsami.5b05097
ACS Appl. Mater. Interfaces 2015, 7, 18662−18671

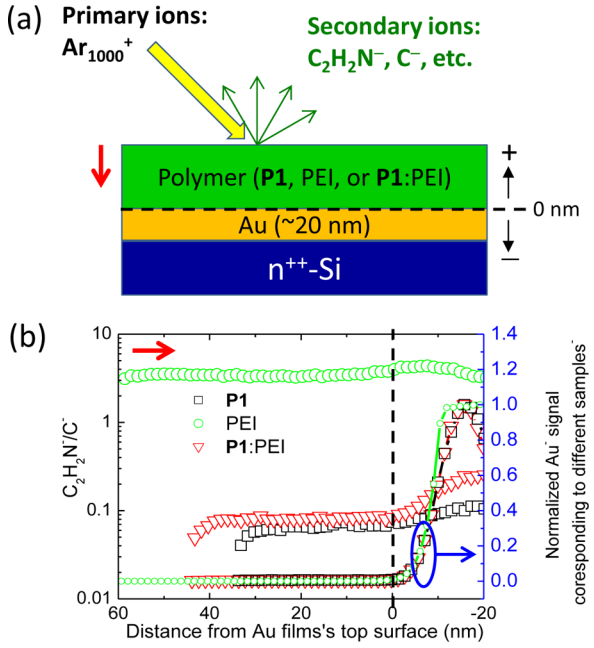

Figure 5. (a) Schematic of the TOF-SIMS measurement by sputtering a thin film of **P1**, PEI or **P1**:PEI (2% PEI) spin-coated on an Au (~20 nm)/n^{++}-Si substrate using argon cluster ions, Ar_{1000}^{+}, with ion beam energy of 5 keV and ion current of 1.8 nA. Positions on, above, and below the Au film's top surface are arbitrarily described be to 0 (horizontal dashed line), positive values, and negative values in units of nm, respectively. The secondary ion species, $C_2H_2N^-$, C^-, and Au^- were detected and analyzed. (b) TOF-SIMS depth profiles of the $C_2H_2N^-/C^-$ ratios of **P1**, PEI and **P1**:PEI (2% PEI) blend films spin-coated on Au/n^{++}-Si substrates as shown in (a). The polymer thin films were annealed at 150 °C for 15 min in nitrogen in a glovebox prior to the measurement. Normalized Au^- signals (on the right *Y* axis) are also shown as depth references and were used to determine the positon of polymer/Au interface (the vertical dashed line at 0 nm).

surface. It can be clearly seen that the $C_2H_2N^-/C^-$ ratio remained almost constant at distances ranging from 0 nm to ~40 nm away from the Au surface. Additionally, the $C_2H_2N^-/C^-$ ratio for the **P1**:PEI film is slightly higher than that of **P1** film throughout. These results suggest that PEI was rather evenly distributed along the vertical direction in the **P1**:PEI blend film. Lower $C_2H_2N^-/C^-$ ratios were obtained in the first few nm on the surface of both **P1** and **P1**:PEI films, which is considered to be due to the lower concentration of liberated secondary ion species that might act as a source of ionizing agents, causing the initial fluctuation of the ion signals.[47,48] Another anomaly is that the $C_2H_2N^-/C^-$ ratios for **P1** and **P1**:PEI films increased dramatically once the Au layer was sputtered, while only slight increases in the actual $C_2H_2N^-$ ion counts within this range were observed (see SI). This could be explained by the stronger absorption of the $C_2H_2N^-$ ions over the C^- ions by the Au film.

AFM images (Figure S6) showed that all the **P1**:PEI blend films containing up to 10% PEI and annealed at high temperatures up to 200 °C are very smooth and uniform (with the root-mean-square roughness (R_q) values <2 nm). At each annealing temperature, a transition from nanofibrils composed of adjoining grains characteristic of pristine **P1** to the more distinct grains in the **P1**:PEI blend films was evident, which likely resulted from the separation of the polymer semiconductor grains by the amorphous PEI phase. With an increased amount of PEI, the excess PEI molecules present at the **P1** grain boundaries would be expected to disrupt the charge transport pathways and decrease the charge carrier mobility, in agreement with the trend observed in Figure 3. In general, the grains became more defined with increasing annealing temperature at each PEI concentration, which is consistent with the dependence of the thin film crystallinity and mobility on the annealing temperature.

The suppression of hole transport observed in **P1** by PEI can be explained by a shift in the Fermi level toward the LUMO due to the electron-donating nitrogen atoms in PEI, similar to the mechanism proposed for the ambipolar-to-n-type conversion of another D−A polymer, P(NDI2OD-T2), in the presence of an n-type dopant $CoCp_2$ or CsF.[36,41] The raised Fermi level of the **P1**:PEI blend would increase the electron concentration but reduce the hole concentration. The increased electron concentration would inhibit hole injection[36,41] and trap injected holes,[38] thereby suppressing hole transport.

Ultraviolet photoelectron spectroscopy (UPS) measurements were conducted on pristine and PEI-doped (2% PEI) **P1** films to determine the Fermi level (E_F) and HOMO level changes (Figure 6). The UPS results confirmed that the **P1** showed an increase in the Fermi level from −4.38 eV to −4.28 eV upon doping with PEI (Table S1). It was also observed that η, the

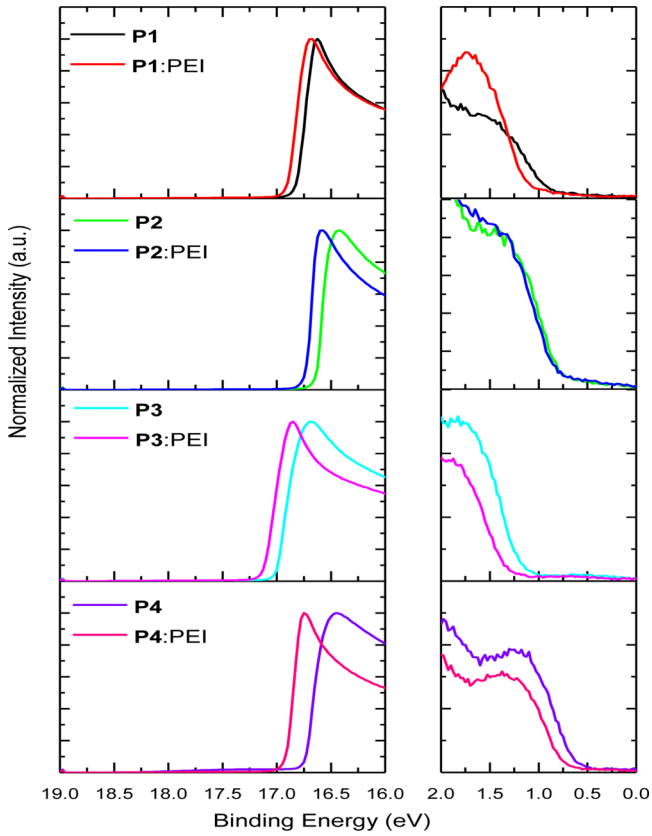

Figure 6. UPS spectra of 150 °C-annealed pristine and 2% PEI doped **P1**, **P2**, **P3**, and **P4** films deposited on Au (30 nm)/n^{++}-Si substrates: Left: the high-energy region showing the secondary electron cut-off (SEC); right: the HOMO region showing the difference between and the Fermi level (at 0 eV) and the HOMO level (curve onset), $\eta = E_F - E_{HOMO}$. After adding PEI, all polymers showed a shift in the Fermi level toward vacuum and an enlarged difference between the HOMO and Fermi level, indicating an n-doping effect of PEI on these polymers.

DOI: 10.1021/acsami.5b05097
ACS Appl. Mater. Interfaces 2015, 7, 18662−18671

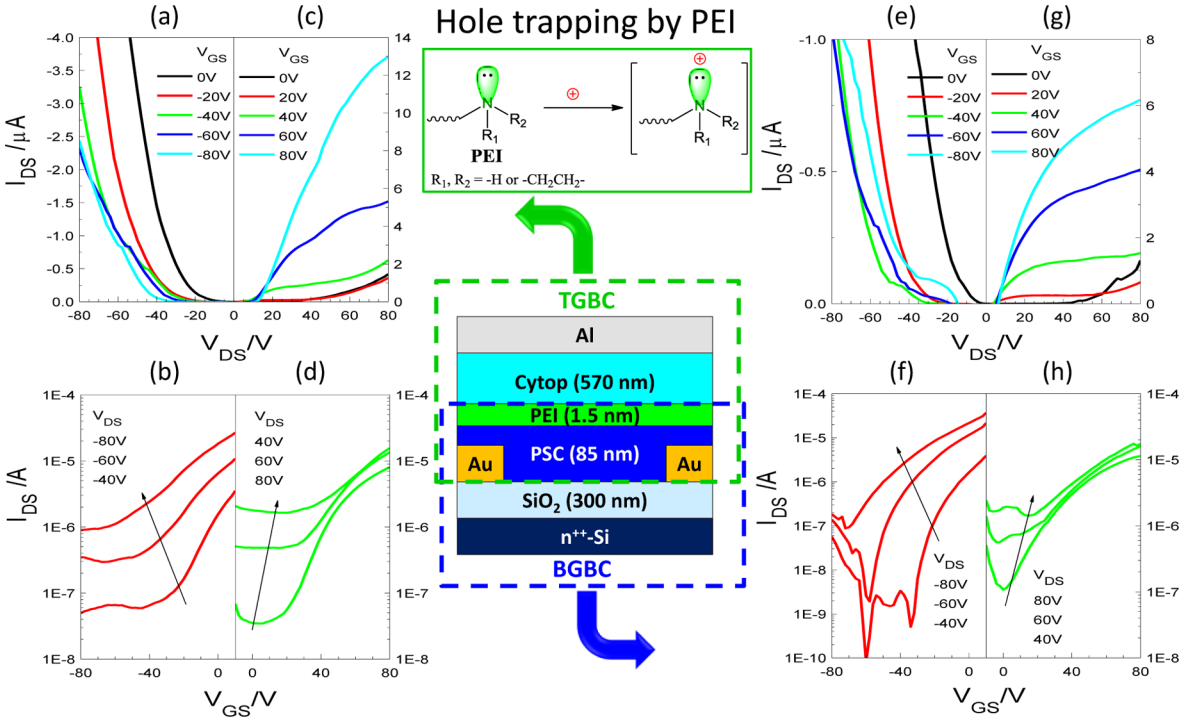

Figure 7. Dual-gate OTFT device containing a TGBC configuration and a BGBC configuration. TGBC configuration: (a) output and (b) transfer characteristics of hole enhancement mode; (c) output and (d) transfer characteristics of electron enhancement mode. BGBC configuration: (e) output and (f) transfer characteristics of hole enhancement mode; (g) output and (h) transfer characteristics of electron enhancement mode. Inserted scheme shows the proposed hole trapping effect of the nitrogen atoms in PEI, which suppresses or eliminates hole transport observed in the TGBC configuration and other devices using the PSC:PEI blends in this study. The PSC is **P1** (annealed at 150 °C) and the SiO_2 surface was modified with dodecyltrichlorosilane (DDTS).

difference between HOMO and E_F, increased from 0.91 to 1.12 eV by PEI doping, similar to the trend observed for the n-doping of pentacene.[44] Since the band gap of **P1** did not change upon PEI doping (see UV−vis spectra in Figure S1), as a result, E_F shifted toward the LUMO level, which is similar to the observation reported for the n-type doping with $CoCp_2$ or CsF.[36,41] The increase in the Fermi level can be ascribed to the filling of electron traps in the polymer semiconductor by the n-type dopant, which can lead to an increase in electron mobility.[36,49,50] At a low PEI content (≤2%), an increase in electron mobility is indeed observed for the **P1**:PEI blends. When the PEI content is greater than 2%, a decrease in electron mobility is observed, which could be attributed to disruptions of the molecular ordering[36] and charge transport pathways by the excess insulating PEI present at the grain boundaries as discussed above.

Another possible contribution to the suppression of hole transport is the work function reduction of the contact electrodes by PEI present in the polymer blend. As observed in our previous studies, a sufficiently reduced work function could block hole injection and suppress the hole transport behavior of ambipolar and p-type polymers.[33,34]

To determine whether PEI promotes hole-trapping, we designed a dual-gate OTFT device using **P1** as the semiconductor on a dodecyltrichlorosilane (DDTS)-modified SiO_2/Si substrate, and Cytop and SiO_2 as the dielectrics for the TGBC and BGBC configurations, respectively. A thin layer of PEI (~1.5 nm) was inserted between the thick polymer semiconductor layer (**P1**, ~85 nm) and the top dielectric Cytop layer (Figure 7). The active layer for the TGBC configuration is the top portion of the **P1** layer adjacent to the PEI layer, while the active layer in the BGBC configuration is the bottom portion of the **P1** layer adjacent to the SiO_2 layer. The purpose of using a rather thick **P1** layer is to prevent the Au source and drain contacts from contacting PEI. In this way, the hole blocking effect due to the work function reduction of Au by PEI can be avoided. Based on the charge transport behavior of these two configurations, we can gain further insight into the hole transport suppression mechanism, i.e., if PEI can trap holes, the TGBC configuration should show weakened or no hole transport performance, whereas the BGBC configuration should still transport holes.

In the hole enhancement mode of the TGBC configuration (Figure 7a, b), the $I-V$ curves show that I_{DS} does not increase when holes accumulate in the top portion of the **P1** as $|V_{GS}|$ increases. The inability to transport holes is caused either by the lack of hole injection from the source or trapping of holes in the top portion of the **P1** layer, which is the active channel of this configuration. By examining the output curve at V_{GS} = 0 V in the electron enhancement mode (Figure 7c), we observe that I_{DS} increases notably with V_{DS} when V_{DS} is >30 V, which confirms that holes were injected from the drain (due to the positive drain-source bias) and transported to the source across the **P1** layer under the V_{DS} bias. This observation infers that the hole transport suppression observed in the hole enhancement mode at V_{GS} > 0 V and V_{DS} > 0 V (Figure 7a, b) was caused by trapping of the holes induced by the negative gate bias in the **P1**and PEI interface and not due to a lack of injected holes. In the electron enhancement mode (Figure 7c, d), the TGBC configuration showed typical electron transport performance with an electron mobility up to 0.12 $cm^2 V^{-1} s^{-1}$ (Table 1). The above data obtained from the TGBC configuration strongly

DOI: 10.1021/acsami.5b05097
ACS Appl. Mater. Interfaces 2015, 7, 18662−18671

indicate that the top portion of the **P1** layer adjacent to the PEI layer is capable of transporting electrons but not holes. It should be noted that a rather high off-current in the electron enhancement mode (Figure 7d) was observed due to hole conduction along the thick ambipolar **P1** layer in the portion far away from the hole-trapping PEI layer.

On the other hand, the BGBC configuration in this dual-gate device showed obvious evidence of hole transport in the hole enhancement mode (Figure 7e, f), confirming that holes were injected from the source and transported to the drain through the bottom portion of **P1** layer adjacent to the SiO_2 interface. The device also exhibited electron transport in the electron enhancement mode ($V_{GS} > 0$ V, $V_{DS} > 0$ V). $\overline{\mu}_e$ and $\overline{\mu}_h$ of the BGBC configuration with the dual-gate structure are 0.023 and 0.0037 $cm^2\ V^{-1}\ s^{-1}$, respectively, which are similar to those (0.067 and 0.020 $cm^2\ V^{-1}\ s^{-1}$) of the BGBC devices with pristine **P1** films built on DDTS-modified SiO_2/Si substrates (Figure S12 and Table S2). The much lower mobilities of BGBC devices on SiO_2/Si substrates than those ($\overline{\mu}_e$ = 0.38 $cm^2\ V^{-1}\ s^{-1}$ and $\overline{\mu}_h$ = 0.29 $cm^2\ V^{-1}\ s^{-1}$) of the **P1**-based TGBC devices shown in Figure 2a might be due to their different dielectric materials and/or the different PSC/dielectric interfacial properties.

Because the TGBC and BGBC configurations in the above dual-gate device exhibited unipolar n-channel and ambipolar device performances, respectively, it can be concluded that PEI promotes hole trapping, which is at least partially attributed to the suppression of hole transport observed in the **P1**:PEI blends (and other PSC blends discussed below), although the work function reduction of Au by PEI present in the PSC:PEI blends might also play a role.

UPS measurements confirmed that polymer semiconductors **P2**, **P3**, and **P4** also showed a shift of the Fermi level toward the vacuum and an increase in the difference between the Fermi level and the HOMO level upon PEI doping (Figure 6 and Table S1), indicating that hole transport suppression of these polymers in OTFTs would also be possible through PEI doping.

We utilized the same device structures for **P1** (Figure 2a, b) to evaluate **P2** and **P3**, which are ambipolar polymers, at an annealing temperature of 150 °C. Both polymers also showed complete suppression of hole transport when the PEI content is greater than 2% (Figure 3). The best electron mobility of 0.084 $cm^2\ V^{-1}\ s^{-1}$ was achieved in a **P2**:PEI blend containing 2% PEI, which is superior to the highest value of 0.063 $cm^2\ V^{-1}\ s^{-1}$ in the ambipolar devices based on pristine **P2** (Table 1). This improvement is probably due to the electron trap-filling effect of PEI discussed previously for the **P1**:PEI blend. For **P3**, the best unipolar n-channel device was also obtained in a **P3**:PEI blend containing 2% PEI that exhibited an electron mobility of 0.95 $cm^2V^{-1}s^{-1}$. However, this electron mobility is lower than that (up to 3.13 $cm^2\ V^{-1}\ s^{-1}$) of the ambipolar devices with pristine **P3**. This drop in electron mobility in the **P3**:PEI blends might be caused by the poor morphology of the blend films (Figure S7). For the **P3**:PEI blend film containing 2% PEI, in particular, many large gaps between grain aggregates formed, which would disrupt the charge hopping between polymer semiconductor grain aggregates.

Pristine **P4** showed typical p-type semiconductor behavior with hole mobility up to 0.58 $cm^2\ V^{-1}\ s^{-1}$ when Au is used as the source/drain contacts (Table 1). When 2% PEI was blended in **P4**, $\overline{\mu}_h$ dropped precipitously to 1.3×10^{-5} $cm^2\ V^{-1}\ s^{-1}$. On the contrary, electron transport behavior with $\overline{\mu}_e$ of 0.024 $cm^2\ V^{-1}\ s^{-1}$ was observed. Hole transport was completely suppressed at a higher PEI content of 10%, but $\overline{\mu}_e$ decreased to 0.0074 $cm^2\ V^{-1}\ s^{-1}$, most likely due to the larger separation of **P4** grains by the increased amount of electrically insulating PEI. Because **P4** showed no electron mobility in its pristine form, the observation of electron transport behavior in the presence of PEI is most likely due to the filling of electron traps by PEI, a similar mechanism proposed to explain the electron transport performance of a poly(2-methoxy-5-2-ethylhexyloxy-1,4-phenylenevinylene (MEH-PPV):decamethylcobaltocene (DMC, an n-type dopant) blend,[35] where the deep electron traps[51] in the polymer semiconductor could be filled by DMC.

4. CONCLUSION

In this study, we successfully demonstrated a facile approach to converting ambipolar and p-type D−A polymer semiconductors into unipolar n-type polymers by adding a small amount of polyethylenimine (PEI) as an n-type dopant to obtain uniform dopant distribution and smooth thin films (with up to 10% PEI and an annealing temperature of 200 °C). The electron-rich nitrogen atoms in PEI are thought to fill the electron traps, raise the Fermi level, and function as trap sites for holes, resulting in unipolar n-channel OTFT performance with improved electron mobility. The method presented here will be very useful in achieving high-performance electron transport organic semiconductors for CMOS logic and other applications such as organic solar cells and thermoelectric devices using readily available ambipolar and even p-type organic semiconductors.

■ ASSOCIATED CONTENT

Supporting Information

The Supporting Information is available free of charge on the ACS Publications website at DOI: 10.1021/acsami.5b05097.

Additional data on UV−vis−NIR, AFM, and OTFT devices (PDF)

■ AUTHOR INFORMATION

Corresponding Author

*E-mail: Yuning.Li@uwaterloo.ca. Tel.: +1 5198884567, ext. 31105.

Author Contributions

The manuscript was written through contributions by all authors. All authors have given approval to the final version of the manuscript.

Funding

This work is supported by the Natural Sciences and Engineering Research Council (NSERC) of Canada (Discovery Grant 402566−2011).

Notes

The authors declare no competing financial interest.

■ ACKNOWLEDGMENTS

The authors thank Dr. Joseph P. Thomas in Waterloo Advanced Technology Lab of University of Waterloo for the TOF-SIMS measurements and discussion.

■ ABBREVIATIONS

PEI, polyethylenimine
OTFTs, organic thin film transistors
OPVs, organic photovoltaics
D, donor

DOI: 10.1021/acsami.5b05097
ACS Appl. Mater. Interfaces 2015, 7, 18662−18671

A, acceptor
CMOS, complementary metal oxide semiconductor
HOMO, highest occupied molecular orbital
LUMO, lowest unoccupied molecular orbital
PSCs, polymer semiconductors
M_w, weight-average molecular weight
M_n, number-average molecular weight
PDI, polydispersity index
UV−vis−NIR, ultraviolet−visible−near-infrared
XRD, X-ray diffractometry
AFM, atomic force microscopy
TOF-SIMS, time-of-flight secondary ion mass spectrometry
UPS, ultraviolet photoelectron spectroscopy
DDTS, dodecyltrichlorosilane
DCB, 1,2-dichlorobenzene
TGBC, top gate bottom contact
BGBC, bottom gate bottom contact
P(NDI2OD-T2), poly[[N,N 9-bis(2-octyldodecyl)-naphthalene-1,4,5,8-bis(dicarboximide)-2,6-diyl]-*alt*-5,59-(2,29-bithiophene)]
R_q, the root-mean-square roughness

REFERENCES

(1) Bundgaard, E.; Krebs, F. C. Low Band Gap Polymers For Organic Photovoltaics. *Sol. Energy Mater. Sol. Cells* **2007**, *91*, 954−985.
(2) Kroon, R.; Lenes, M.; Hummelen, J. C.; Blom, P. W. M.; de Boer, B. Small Bandgap Polymers for Organic Solar Cells (Polymer Material Development in the Last 5 Years). *Polym. Rev.* **2008**, *48*, 531−582.
(3) Facchetti, A. π-Conjugated Polymers for Organic Electronics and Photovoltaic Cell Applications. *Chem. Mater.* **2010**, *23*, 733−758.
(4) Chen, J.; Cao, Y. Development of Novel Conjugated Donor Polymers for High-Efficiency Bulk-Heterojunction Photovoltaic Devices. *Acc. Chem. Res.* **2009**, *42*, 1709−1718.
(5) Kularatne, R. S.; Magurudeniya, H. D.; Sista, P.; Biewer, M. C.; Stefan, M. C. Donor−acceptor Semiconducting Polymers For Organic Solar Cells. *J. Polym. Sci., Part A: Polym. Chem.* **2013**, *51*, 743−768.
(6) Li, Y.; Sonar, P.; Murphy, L.; Hong, W. High Mobility Diketopyrrolopyrrole (DPP)-based Organic Semiconductor Materials For Organic Thin Film Transistors And Photovoltaics. *Energy Environ. Sci.* **2013**, *6*, 1684−1710.
(7) He, Y.; Hong, W.; Li, Y. New Building Blocks For π-Conjugated Polymer Semiconductors For Organic Thin Film Transistors And Photovoltaics. *J. Mater. Chem. C* **2014**, *2*, 8651−8661.
(8) Guo, C.; Hong, W.; Aziz, H.; Li, Y. Recent Progress in High Mobility Polymer Semiconductors for Organic Thin Film Transistors. *Rev. Adv. Sci. Eng.* **2012**, *1*, 200−224.
(9) Nielsen, C. B.; Turbiez, M.; McCulloch, I. Recent Advances in the Development of Semiconducting DPP-Containing Polymers for Transistor Applications. *Adv. Mater.* **2013**, *25*, 1859−1880.
(10) Liu, Y.; Zhao, J.; Li, Z.; Mu, C.; Ma, W.; Hu, H.; Jiang, K.; Lin, H.; Ade, H.; Yan, H. Aggregation and Morphology Control Enables Multiple Cases of High-efficiency Polymer Solar Cells. *Nat. Commun.* **2014**, *5*, 5293.
(11) Li, J.; Zhao, Y.; Tan, H. S.; Guo, Y.; Di, C.-A.; Yu, G.; Liu, Y.; Lin, M.; Lim, S. H.; Zhou, Y.; Su, H.; Ong, B. S. A Stable Solution-processed Polymer Semiconductor With Record High-mobility for Printed Transistors. *Sci. Rep.* **2012**, *2*, 754.
(12) Kang, I.; Yun, H. J.; Chung, D. S.; Kwon, S. K.; Kim, Y. H. Record High Hole Mobility in Polymer Semiconductors via Side-Chain Engineering. *J. Am. Chem. Soc.* **2013**, *135*, 14896−14899.
(13) Kim, G.; Kang, S. J.; Dutta, G. K.; Han, Y. K.; Shin, T. J.; Noh, Y. Y.; Yang, C. A Thienoisoindigo-Naphthalene Polymer with Ultrahigh Mobility of 14.4 $cm^2/V{\cdot}s$ That Substantially Exceeds Benchmark Values for Amorphous Silicon Semiconductors. *J. Am. Chem. Soc.* **2014**, *136*, 9477−9483.
(14) Baker, R. J. *CMOS: Circuit Design, Layout, and Simulation*, 3rd ed.;Tewksbury, S. K.; Brewer, J. E., Eds.; John Wiley & Sons: Hoboken, NJ, 2010; Chapter 1, pp 6−7.
(15) Baeg, K. J.; Caironi, M.; Noh, Y. Y. Toward Printed Integrated Circuits based on Unipolar or Ambipolar Polymer Semiconductors. *Adv. Mater.* **2013**, *25*, 4210−4244.
(16) Zhao, X.; Zhan, X. Electron Transporting Semiconducting Polymers in Organic Electronics. *Chem. Soc. Rev.* **2011**, *40*, 3728−3743.
(17) Bürgi, L.; Turbiez, M.; Pfeiffer, R.; Bienewald, F.; Kirner, H.-J.; Winnewisser, C. High-Mobility Ambipolar Near-Infrared Light-Emitting Polymer Field-Effect Transistors. *Adv. Mater.* **2008**, *20*, 2217−2224.
(18) Bijleveld, J. C.; Zoombelt, A. P.; Mathijssen, S. G. J.; Wienk, M. M.; Turbiez, M.; de Leeuw, D. M.; Janssen, R. A. J. Poly(diketopyrrolopyrrole-terthiophene) for Ambipolar Logic and Photovoltaics. *J. Am. Chem. Soc.* **2009**, *131*, 16616−16617.
(19) Sonar, P.; Singh, S. P.; Li, Y.; Soh, M. S.; Dodabalapur, A. A Low-Bandgap Diketopyrrolopyrrole-Benzothiadiazole-Based Copolymer for High-Mobility Ambipolar Organic Thin-Film Transistors. *Adv. Mater.* **2010**, *22*, 5409−5413.
(20) Yuen, J. D.; Fan, J.; Seifter, J.; Lim, B.; Hufschmid, R.; Heeger, A. J.; Wudl, F. High Performance Weak Donor-Acceptor Polymers in Thin Film Transistors: Effect of the Acceptor on Electronic Properties, Ambipolar Conductivity, Mobility, and Thermal Stability. *J. Am. Chem. Soc.* **2011**, *133*, 20799−20807.
(21) Hong, W.; Sun, B.; Aziz, H.; Park, W. T.; Noh, Y. Y.; Li, Y. N. A Conjugated Polyazine Containing Diketopyrrolopyrrole for Ambipolar Organic Thin Film Transistors. *Chem. Commun.* **2012**, *48*, 8413−8415.
(22) Hong, W.; Sun, B.; Yuen, J.; Li, Y. N.; Lu, S. F.; Huang, C.; Facchetti, A. Dipyrrolo[2,3-b:2′,3′-e]pyrazine-2,6(1H,5H)-dione Based Conjugated Polymers for Ambipolar Organic Thin-film Transistors. *Chem. Commun.* **2013**, *49*, 484−486.
(23) Lee, J.; Han, A. R.; Yu, H.; Shin, T. J.; Yang, C.; Oh, J. H. Boosting the Ambipolar Performance of Solution-Processable Polymer Semiconductors via Hybrid Side-Chain Engineering. *J. Am. Chem. Soc.* **2013**, *135*, 9540−9547.
(24) Sun, B.; Hong, W.; Yan, Z.; Aziz, H.; Li, Y. Record High Electron Mobility of 6.3 $cm^2V^{-1}s^{-1}$ Achieved for Polymer Semiconductors Using a New Building Block. *Adv. Mater.* **2014**, *26*, 2636−2642.
(25) Bisri, S. Z.; Piliego, C.; Gao, J.; Loi, M. A. Outlook and Emerging Semiconducting Materials for Ambipolar Transistors. *Adv. Mater.* **2014**, *26*, 1176−1199.
(26) Bronner, M.; Opitz, A.; Brütting, W. Ambipolar Charge Carrier Transport in Organic Semiconductor Blends of Phthalocyanine and Fullerene. *Phys. Status Solidi A* **2008**, *205*, 549−563.
(27) Xu, H.; Zhou, Y.-C.; Zhou, X.-Y.; Liu, K.; Cao, L.-Y.; Ai, Y.; Fan, Z.-P.; Zhang, H.-L. Molecular Packing-Induced Transition between Ambipolar and Unipolar Behavior in Dithiophene-4,9-dione-Containing Organic Semiconductors. *Adv. Funct. Mater.* **2014**, *24*, 2907−2915.
(28) Ribierre, J. C.; Watanabe, S.; Matsumoto, M.; Muto, T.; Aoyama, T. Majority Carrier Type Conversion in Solution-processed Organic Transistors and Flexible Complementary Logic Circuits. *Appl. Phys. Lett.* **2010**, *96*, 083303.
(29) Ribierre, J.-C.; Watanabe, S.; Matsumoto, M.; Muto, T.; Nakao, A.; Aoyama, T. Reversible Conversion of the Majority Carrier Type in Solution-Processed Ambipolar Quinoidal Oligothiophene Thin Films. *Adv. Mater.* **2010**, *22*, 4044−4048.
(30) Cheng, X.; Noh, Y.-Y.; Wang, J.; Tello, M.; Frisch, J.; Blum, R.-P.; Vollmer, A.; Rabe, J. P.; Koch, N.; Sirringhaus, H. Controlling Electron and Hole Charge Injection in Ambipolar Organic Field-Effect Transistors by Self-Assembled Monolayers. *Adv. Funct. Mater.* **2009**, *19*, 2407−2415.
(31) Baeg, K.-J.; Kim, J.; Khim, D.; Caironi, M.; Kim, D.-Y.; You, I.-K.; Quinn, J. R.; Facchetti, A.; Noh, Y.-Y. Charge Injection Engineering of Ambipolar Field-Effect Transistors for High-Performance Organic Complementary Circuits. *ACS Appl. Mater. Interfaces* **2011**, *3*, 3205−3214.

DOI: 10.1021/acsami.5b05097
ACS Appl. Mater. Interfaces 2015, 7, 18662−18671

(32) Zhou, Y.; Fuentes-Hernandez, C.; Shim, J.; Meyer, J.; Giordano, A. J.; Li, H.; Winget, P.; Papadopoulos, T.; Cheun, H.; Kim, J.; Fenoll, M.; Dindar, A.; Haske, W.; Najafabadi, E.; Khan, T. M.; Sojoudi, H.; Barlow, S.; Graham, S.; Brédas, J.-L.; Marder, S. R.; Kahn, A.; Kippelen, B. A Universal Method to Produce Low−Work Function Electrodes for Organic Electronics. *Science* **2012**, *336*, 327−332.
(33) Sun, B.; Hong, W.; Thibau, E.; Aziz, H.; Lu, Z.-H.; Li, Y. Facile Conversion of Polymer Organic Thin Film Transistors From Ambipolar and p-Type into Unipolar n-Type Using Polyethyleneimine (PEI)-modified Electrodes. *Org. Electron.* **2014**, *15*, 3787−3794.
(34) Sun, B.; Hong, W.; Aziz, H.; Li, Y. A Pyridine-flanked Diketopyrrolopyrrole (DPP)-based Donor-acceptor Polymer Showing High Mobility in Ambipolar and N-channel Organic Thin Film Transistors. *Polym. Chem.* **2015**, *6*, 938−945.
(35) Zhang, Y.; de Boer, B.; Blom, P. W. M. Trap-free Electron Transport in Poly(p-phenylene vinylene) by Deactivation of Traps with n-Type Doping. *Phys. Rev. B: Condens. Matter Mater. Phys.* **2010**, *81*, 085201.
(36) Liu, C.; Jang, J.; Xu, Y.; Kim, H.-J.; Khim, D.; Park, W.-T.; Noh, Y.-Y.; Kim, J.-J. Effect of Doping Concentration on Microstructure of Conjugated Polymers and Characteristics in N-Type Polymer Field-Effect Transistors. *Adv. Funct. Mater.* **2015**, *25*, 758−767.
(37) Wei, P.; Oh, J. H.; Dong, G.; Bao, Z. Use of a 1H-Benzoimidazole Derivative as an n-Type Dopant and To Enable Air-Stable Solution-Processed n-Channel Organic Thin-Film Transistors. *J. Am. Chem. Soc.* **2010**, *132*, 8852−8853.
(38) Naab, B. D.; Himmelberger, S.; Diao, Y.; Vandewal, K.; Wei, P.; Lussem, B.; Salleo, A.; Bao, Z. High Mobility N-Type Transistors Based on Solution-Sheared Doped 6,13-Bis(triisopropylsilylethynyl)-pentacene Thin Films. *Adv. Mater.* **2013**, *25*, 4663−4667.
(39) Naab, B. D.; Zhang, S.; Vandewal, K.; Salleo, A.; Barlow, S.; Marder, S. R.; Bao, Z. Effective Solution- and Vacuum-Processed n-Doping by Dimers of Benzimidazoline Radicals. *Adv. Mater.* **2014**, *26*, 4268−4272.
(40) Naab, B. D.; Guo, S.; Olthof, S.; Evans, E. G. B.; Wei, P.; Millhauser, G. L.; Kahn, A.; Barlow, S.; Marder, S. R.; Bao, Z. Mechanistic Study on the Solution-Phase n-Doping of 1,3-Dimethyl-2-aryl-2,3-dihydro-1H-benzoimidazole Derivatives. *J. Am. Chem. Soc.* **2013**, *135*, 15018−15025.
(41) Khim, D.; Baeg, K.-J.; Caironi, M.; Liu, C.; Xu, Y.; Kim, D.-Y.; Noh, Y.-Y. Control of Ambipolar and Unipolar Transport in Organic Transistors by Selective Inkjet-Printed Chemical Doping for High Performance Complementary Circuits. *Adv. Funct. Mater.* **2014**, *24*, 6252−6261.
(42) Sun, B.; Hong, W.; Aziz, H.; Abukhdeir, N. M.; Li, Y. Dramatically Enhanced Molecular Ordering and Charge Transport of a DPP-based Polymer Assisted by Oligomers Through Antiplasticization. *J. Mater. Chem. C* **2013**, *1*, 4423−4426.
(43) Thomas, J. P.; Leung, K. T. Defect-Minimized PEDOT:PSS/Planar-Si Solar Cell with Very High Efficiency. *Adv. Funct. Mater.* **2014**, *24*, 4978−4985.
(44) Lüssem, B.; Tietze, M. L.; Kleemann, H.; Hoßbach, C.; Bartha, J. W.; Zakhidov, A.; Leo, K. Doped Organic Transistors Operating in the Inversion and Depletion Regime. *Nat. Commun.* **2013**, *4*, 2775.
(45) Jones, B. A.; Facchetti, A.; Wasielewski, M. R.; Marks, T. J. Tuning Orbital Energetics in Arylene Diimide Semiconductors. Materials Design for Ambient Stability of n-Type Charge Transport. *J. Am. Chem. Soc.* **2007**, *129*, 15259−15278.
(46) Yan, H.; Chen, Z.; Zheng, Y.; Newman, C.; Quinn, J. R.; Dotz, F.; Kastler, M.; Facchetti, A. A High-mobility Electron-transporting Polymer for Printed Transistors. *Nature* **2009**, *457*, 679−686.
(47) Mahoney, C. M. Cluster Secondary Ion Mass Spectrometry of Polymers and Related Materials. *Mass Spectrom. Rev.* **2010**, *29*, 247−293.
(48) Wucher, A. Molecular Secondary Ion Formation under Cluster Bombardment: A Fundamental Review. *Appl. Surf. Sci.* **2006**, *252*, 6482−6489.
(49) Ma, L.; Lee, W. H.; Park, Y. D.; Kim, J. S.; Lee, H. S.; Cho, K. High Performance Polythiophene Thin-film Transistors Doped with Very Small Amounts of an Electron Acceptor. *Appl. Phys. Lett.* **2008**, *92*, 063310.
(50) Olthof, S.; Mehraeen, S.; Mohapatra, S. K.; Barlow, S.; Coropceanu, V.; Brédas, J.-L.; Marder, S. R.; Kahn, A. Ultralow Doping in Organic Semiconductors: Evidence of Trap Filling. *Phys. Rev. Lett.* **2012**, *109*, 176601.
(51) Nicolai, H. T.; Kuik, M.; Wetzelaer, G. A. H.; de Boer, B.; Campbell, C.; Risko, C.; Brédas, J. L.; Blom, P. W. M. Unification of Trap-limited Electron Transport in Semiconducting Polymers. *Nat. Mater.* **2012**, *11*, 882−887.
(52) Li, Y.; Sonar, P.; Singh, S. P.; Soh, M. S.; van Meurs, M.; Tan, J. Annealing-Free High-Mobility Diketopyrrolopyrrole-Quaterthiophene Copolymer for Solution-Processed Organic Thin Film Transistors. *J. Am. Chem. Soc.* **2011**, *133*, 2198−2204.

DOI: 10.1021/acsami.5b05097
ACS Appl. Mater. Interfaces 2015, 7, 18662−18671